Monoenergetic Proton Beams Accelerated by a Radiation Pressure Driven Shock

Charlotte A. J. Palmer,[1] N. P. Dover,[1] I. Pogorelsky,[2] M. Babzien,[2] G. I. Dudnikova,[3] M. Ispiriyan,[4] M. N. Polyanskiy,[2] J. Schreiber,[1,5,6] P. Shkolnikov,[4] V. Yakimenko,[2] and Z. Najmudin[1]

[1]*Blackett Laboratory, Imperial College, London SW7 2AZ, United Kingdom*
[2]*Accelerator Test Facility, Brookhaven National Laboratory, Upton, New York 11973, USA*
[3]*University of Maryland, College Park, Maryland 20742, USA*
[4]*Stony Brook University, Stony Brook, New York 11794, USA*
[5]*Fakultät für Physik, Ludwig-Maximilians-Universität München, D-85748 Garching, Germany*
[6]*Max-Planck-Institut für Quantenoptik, Hans-Kopfermann-Straße 1, D-85748 Garching, Germany*

(Received 19 October 2010; published 4 January 2011)

We report on the acceleration of impurity-free quasimononenergetic proton beams from an initially gaseous hydrogen target driven by an intense infrared ($\lambda = 10\ \mu$m) laser. The front surface of the target was observed by optical probing to be driven forward by the radiation pressure of the laser. A proton beam of ~MeV energy was simultaneously recorded with narrow energy spread ($\sigma \sim 4\%$), low normalized emittance (~ 8 nm), and negligible background. The scaling of proton energy with the ratio of intensity over density (I/n) confirms that the acceleration is due to the radiation pressure driven shock.

DOI: 10.1103/PhysRevLett.106.014801 PACS numbers: 41.75.Jv

High intensity lasers can accelerate ion beams from plasmas to high energies (> MeV) in extremely short distances (< 100 μm). Most investigations of ion acceleration by intense lasers have relied on sheath acceleration [1–3]. When a high-intensity laser impacts on a solid target, an overdense (opaque) plasma is formed ($n_e > n_{\mathrm{cr}} = \epsilon_0 m\omega_0^2/e^2$). Laser energy is converted into hot electrons with temperature $k_B T_e$, which form an electrostatic sheath around the target with fields $\gtrsim \mathrm{MV}/\mu\mathrm{m}$. The sheath accelerates surface ions to energies $\approx k_B T_e$ (~ multi-MeV) per nucleon [4]. However, ions are usually emitted from both the front and back surface with a broad energy spread and a number of ion species present, many originating from impurities [3,5]. Furthermore, the ion energy scales poorly with irradiance [$\sim (I\lambda^2)^{1/2}$] [6]. Modulated ion energy spectra have been produced, by using complex targets [7], or energy selection [8], but these methods feature poor peak-to-noise spectral contrast, low yields, and the presence of multiple species.

Radiation-pressure acceleration (RPA) has been proposed as an alternative method of ion acceleration at ultrahigh intensities [9–12]. For an opaque plasma ($n_e > n_{\mathrm{cr}}$), radiation pressure, $P_R = 2I/c$, pushes electrons into the target, setting up an electrostatic shock whose space charge field pulls along ions at the hole-boring velocity, $v_{\mathrm{hb}} \approx (2I/\rho c)^{1/2}$, where I is the intensity and ρ the mass density [13]. Stationary ions in advance of the shock front "bounce" off the electrostatic field associated with the shock, producing a population of energetic ions with velocity $2v_{\mathrm{hb}}$ [14]. If the target becomes sufficiently thin so that all of the electrons are pushed out of the target ($d < c/\omega_p$), the ions can be pulled along in unison in the "light-sail" phase of RPA, which allows higher energy to be reached [12]. First experiments have now reported limited enhancement of ion energy contrast with optical lasers and ultrathin solid targets [15]. However, due to the high intensities required and high densities used, energy gains were modest, energy spreads large, and yields low, especially for protons due to the presence of multiple species. The ultrathin targets also require exceptionally high laser contrast between main pulse and preceding prepulse, since solids are particularly susceptible to ionization and deformation even at modest intensities [16].

Gas targets are an alternative to solid foils. They operate at high-repetition rate, are easily adjusted for target density and material, are less prone to contamination, and less susceptible to prepulse [17]. However, they are difficult to operate at near or above critical density, which is necessary for efficient ion acceleration (e.g., for 1 μm laser, $n_{\mathrm{crit}} \simeq 1 \times 10^{21}\ \mathrm{cm}^{-3}$) [18]. This can be remedied by use of longer wavelength lasers. For example, for a $\lambda \approx 10\ \mu$m infrared CO_2 laser, $n_{\mathrm{crit}} (\propto \lambda^{-2}) \approx 10^{19}\ \mathrm{cm}^{-3}$. This density is easily obtained by ionization of gas targets. Importantly, due to the lower specific mass ($< 10^4 \times$ solid densities), gas targets become of interest for RPA at proportionally reduced laser intensity.

In this Letter, we show that the interaction of an intense far-infrared laser with a gaseous hydrogen target can produce radiation-pressure effects at intensities $I < 10^{16}\ \mathrm{W\,cm}^{-2}$, many orders of magnitude ($\ll 1000$) less than with optical lasers [15]. Narrow-energy-spread impurity-free proton beams were produced whose energies scale with the ratio of intensity over density (I/n), indicating that the acceleration is due to the shock generated by radiation-pressure driven hole boring of the critical surface [13]. The propagation of the shock into the target is directly observed by optical probing.

The experiment was performed using the $\lambda = 10\ \mu$m, 0.5 TW peak power, circularly polarized CO_2 laser at the Accelerator Test Facility, Brookhaven National Laboratory. The short pulse is achieved in a Kerr cell filled with optically active CS_2 liquid via fast polarization switching using a 5 ps long, frequency-doubled ($\lambda =$ 532 nm) Nd:YAG beam. Spectral modulation of a picosecond $\lambda = 10\ \mu$m pulse in CO_2 gas amplifiers results in splitting of the output pulse into a train of 6 ps pulses with 25 ps period with most of the energy (on average 70%) contained in two leading pulses. This was monitored on every shot with a streak camera, with the most intense pulse containing $42 \pm 8\%$ of the total energy. The variation in this ratio gave the largest uncertainty in intensity. Shots were taken with integrated energy in the range 2.5–2.9 J and focused by an $f/3$ off-axis parabolic mirror to a spot size of $w_0 \approx 70\ \mu$m. This gives vacuum target intensities of $5.4\text{–}6.3 \times 10^{15}(\pm 14\%)$ W cm^{-2}, or normalized vector potential $a_0 \simeq 0.47\text{–}0.51$, where for circular polarization $a_0 = eE/m\omega c \simeq 0.60(I\lambda^2)^{1/2}$ (for I in 10^{18} W cm^{-2} and λ in μm). This would imply a hot electron temperature $k_B T_e \sim U_p \sim 100$'s keV, where $U_p \equiv a_0^2 m_e c^2$ is the ponderomotive potential. This could promote sheath acceleration, but was mitigated to some extent by use of circular polarization [10,19].

The laser was focused onto the front surface of a hydrogen gas jet from a 1 mm opening diameter circular nozzle. The interaction was diagnosed by transverse probing and measurements of the forward accelerated ion beam. A $\tau =$ 5 ps, 2ω ($\lambda = 532$ nm) Nd:YAG laser beam, synchronized with the CO_2 beam, was used for probing. The relative timing between driver and probe pulse was varied using an optical delay line. The probe, after passing orthogonal to the infrared beam through the plasma, was split and directed into shadowgraphy and interferometry channels. These gave information about plasma creation and evolution, and also provided the *in situ* neutral density profile. Density information was obtained from the interferograms, by first obtaining the phase with reference to a background image. An Abel transform was then used to obtain the density profile from the phase change, assuming cylindrical symmetry around the laser axis. Along the optical axis, ~0.7 mm above the nozzle edge, the density was found to have an approximately triangular density profile, going from zero to maximum density over a length of $\approx 825\ \mu$m. The density of hydrogen atoms could be varied up to a maximum of $n \sim 10^{20}$ cm$^{-3} \simeq 10 n_{cr}$. Note that for hydrogen $n = n_e$. Probing just before arrival of the CO_2 pulse train shows no sign of preionization of the target, implying a laser contrast $>10^3$.

The ion beam was characterized with a magnetic spectrometer, which dispersed the protons by their deflection in a transverse magnetic field. The aperture of the spectrometer was a $\phi = 0.6$ mm diameter pinhole. The dispersed protons were detected with a polyvinyltoluene scintillator screen whose light emission was calibrated to the dose of energy deposited by protons. The scintillator was imaged on to an Andor EMCCD camera.

Figure 1 shows a selection of ion beams recorded with the magnetic spectrometer for a range of densities and intensities. Ion beams with a peak energy up to $E_{max} =$ 1.1 MeV were observed. The most striking observation is the narrow spectral width of the ion features, especially at higher I/n. All of the beams recorded in this run were found to have peaked spectra. Though the energy spread varies, for the ion beam shown in Fig. 1(a), the image is a circle comparable in size to the projected aperture size at the image plane, indicating that this feature is dominated by the instrument function of the spectrometer. Proton energy spectra were unfolded by first removing hot spots (due to x rays), background subtracting, and then integrating vertically to give a lineout. An absolute residuals optimization was used to find the trial spectra which best reproduced the measured signal after convolving with the instrument function, which was taken from the vertical spread of the signal. Because of its small acceptance angle (9.8×10^{-6} sr), transport through the spectrometer has

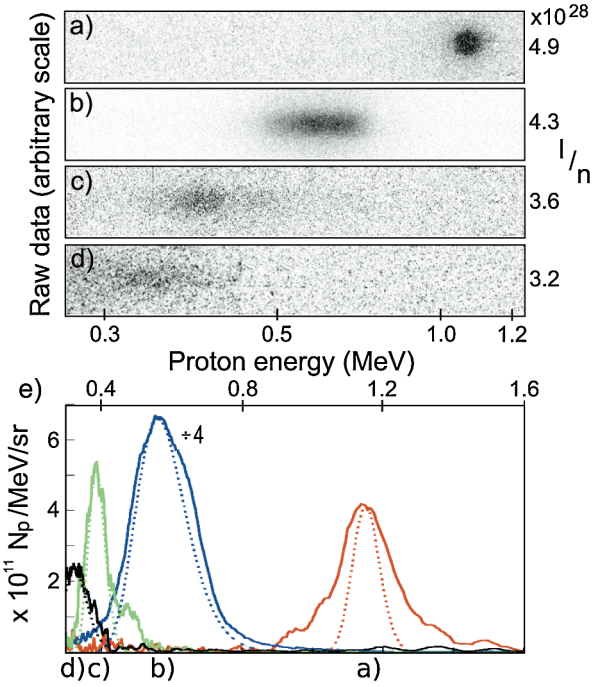

FIG. 1 (color online). Raw and processed proton spectra for varying peak density n and vacuum intensity I showing scaling of peak proton energy $E_{max} \propto I/nc$ [MeV]. Parameter I/n shown to the right of the respective raw images. Shots taken with (a) $I = 6.4$, $n = 6.1 n_{cr}$, (b) $I = 5.5$, $n = 6.1 n_{cr}$, (c) $I = 5.9$, $n = 7.6 n_{cr}$, (d) $I = 5.7$, $n = 8.0 n_{cr}$ (I in units of 10^{15} W cm^{-2}). (e) Background subtracted (solid lines) and also corrected (dashed lines) spectra. Heights of corrected spectra adjusted to match those of raw lineouts. Lineout corresponding to (b) reduced 4× to fit on the same scale.

little effect on the signal spread. The deconvolved spectra [Fig. 1(e)] show that the narrowest observed feature [Fig. 1(a)] corresponds to an rms energy spread of only $\sigma = 4.2\%$. The peak-to-noise contrast of the spectrum is >100, which was limited by detector sensitivity.

For the shot peaking at 0.6 MeV [Fig. 1(b)], the maximum of the spectrum is $\sim 3 \times 10^{12}$ protons/MeV/sr (note that the scale for this trace should be $\times 4$), which is at least >300 times greater than for previously reported quasimonoenergetic ion beams from laser accelerators [7,15]. From the transverse spread of the 4×10^6 protons passing through the spectrometer pinhole, the geometrical emittance of the beam was determined to be $\epsilon = 0.16$ mm mrad, corresponding to a normalized emittance of $\epsilon_n \equiv \beta\gamma\epsilon = 8$ nm rad.

Also apparent is that the peak energy increases with increasing I/n over this density range. This is shown more clearly in Fig. 2, which plots measured peak energy versus expected energy due to shock acceleration, $E = \frac{1}{2}m(2v_{\mathrm{hb}})^2 = 4I/nc$. Note that this includes data both with the same intensity I, but varying n, and also constant n but varying I. Despite a relatively large shot-to-shot variability, which appears to be correlated to the variability in energy balance between pulses in the pulse train, the data show a clear trend of increasing energy for increasing I/n. A linear trend line demonstrating a scaling with I/n is given for comparison in Fig. 2. However, this trend line is for values of I/n eleven times higher than expected by taking the vacuum focused intensity and the peak measured densities. This discrepancy will be addressed further below. The vertical bars in Fig. 2 represent the rms energy spread, emphasizing that all of these beams have narrow energy spread.

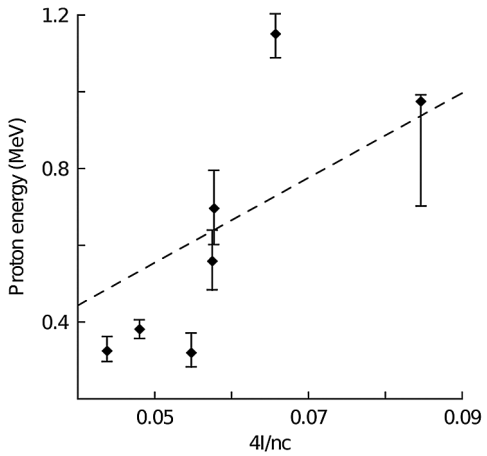

FIG. 2. Proton energy scaling as a function of expected energy due to hole boring, $E = 4I/nc$. For $8n_{\mathrm{cr}} > n > 4n_{\mathrm{cr}}$, peak proton signal increases with increasing I/n. For $n < 4n_{\mathrm{cr}}$ beams were produced with larger variation in energy (below the observed scaling), and are not included. No beams observed above detector limit for $n > 8n_{\mathrm{cr}}$. Vertical bars represent rms energy spread of each shot.

Although opaque to the infrared driver, the plasma at these densities is transparent at optical wavelengths, allowing direct probing. By contrast, probing the surface of a solid-density interaction would be impossible due to severe refraction. Figure 3(a) shows a shadowgram of an interaction for peak density $n = 4n_{\mathrm{cr}}$, at $t \sim 30$ ps after arrival of the main CO_2 pulse, shortly after the end of the interaction with the second pulse. A cavity has been created by the laser inside the gas target. Simultaneous interferometry shows that the plasma within the cavity is at much lower density ($< 10^{18}$ cm^{-3}), while the walls of the cavity are just above critical density. Hence this density-discontinuity (shock) is associated with hole-boring. The laser has traveled to the critical surface, where it is mostly reflected. The resultant radiation pressure causes the critical surface to be driven inwards. The shock front has moved about 250 μm since the end of the pulse, giving an initial velocity of $\sim 10^7$ ms^{-1}, which is consistent with v_{hb} inferred from the ion energies. Probing at later times [Fig. 3(b)] shows the shock front moving further into the target, though at reduced velocity due to dissipation of the shock energy. We note that even at these late times, the motion of the back surface is barely perceptible, suggesting that sheath accelerated ions would be of too low energy to be detected.

To model the interaction, 2D particle-in-cell simulations were performed with the code OSIRIS [20], using $20\,000 \times 3000$ cells to simulate a 600×500 μm ($\sim 60 \times 50\lambda$) box. The laser was incident on fully ionized hydrogen plasma with density profile increasing from 0 to $7.5n_c$ in 100 μm. The parameters were chosen to replicate the experiment ($a_0 = 0.6$, $\tau_L = 8$ ps $= 229$ laser periods, circular polarization). A hole-boring front can be seen [Fig. 4(a)] forming at a density initially between n_{cr} and $2n_{\mathrm{cr}}$—well below the peak density. Though the target is only $L \approx 100\lambda$, it is not thin enough for "light-sail" RPA, with the shock front traveling $<10\lambda$ during the laser duration. The velocity of the front increases up to the peak of the laser pulse where it is comparable to the expected hole-boring velocity, v_{hb} for the local interaction density. The velocity of the hole-boring front is found to decrease as the peak density of

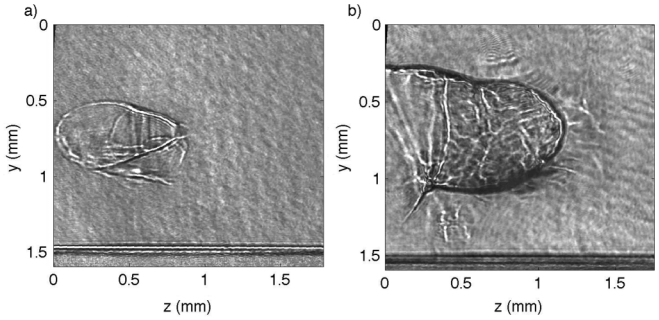

FIG. 3. Shadowgraphy of the interaction for $n = 4n_{\mathrm{cr}}$ at (a) ~ 30 ps and (b) 200 ps after the first main pulse interacts with the gas. Laser entered from left, with the silhouette of the gas nozzle shown below.

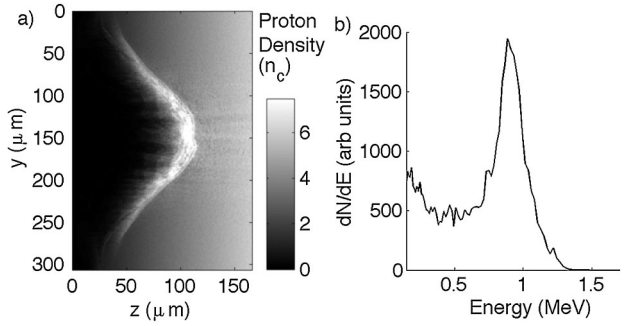

FIG. 4. PIC simulation showing (a) Proton density map and (b) proton spectra as seen by simulated spectrometer taken 12 ps after the start of the interaction.

the profile is increased. This is because the shock, though starting at $n \sim n_{cr}$, meets a higher density as it moves forward. Simulations with double pulses show that the secondary pulses enhance the shock structure and snowplow a greater number of protons to v_{hb}. However, the maximum ion energies are always determined by $2v_{hb}$ of the more intense pulse.

The simulations also show self-focusing of the laser pulses (by $>2\times$ in intensity) [21]. In conjunction with the lower than peak interaction density, this explains the previously noted experimental discrepancy between measured and predicted ion energies. The nonlinear response of self-focusing would also be likely to cause variations in ion beam properties. Self-focusing is accentuated in three dimensions. To account for this a further simulation was performed with $a_0 = 0.9$ and shorter density scale length. Figure 4(b) shows the spectrum observed in a simulated spectrometer with the same acceptance angle as in the experiment. A sharp peak is observed at high energy, in the energy range observed experimentally. In momentum phase space, the peak can be clearly identified with a population of ions traveling ahead of the shock front at $v = 2v_{hb}$. Assuming a real beam divergence comparable to that of the simulated high energy proton bunch ($\sim 4°$) would imply a total of up to 5×10^9 ($\simeq 0.8$ nC) in the accelerated proton bunch.

Though ion acceleration with CO_2 lasers was extensively studied [1], the use of gas targets represents a conceptual advance. Not only does it allow the acceleration of impurity-free proton beams, it also allows the exploration of RPA schemes at greatly reduced intensity. Even at $I < 10^{16}$ W cm^{-2}, proton beams are observed with properties far superior to previous measurements of laser generated quasimonoenergetic ion beams [7,15]. These properties include small energy spread ($\sigma \sim 4\%$), low background ($> 100\times$ contrast), and high spectral brightness ($> 10^{12}$ protons/MeV/sr). These are the first background free proton beams produced by radiation-pressure effects. Further simulations at higher intensity have reiterated the favorable scaling for over an order of magnitude increase laser intensity ($\propto I$ at mildly relativistic intensities), suggesting it should be straightforward to achieve energies comparable to other laser-driven ion schemes. This coupled to the use of a target that naturally lends itself to high-repetition rate usage, makes it possible to envisage producing the high-current, low-energy spread, impurity-free proton beams that could fulfill the promise of plasma based acceleration schemes.

The work was funded in part by Libra Basic Tech. and U.S. DOE Grant No. DE-FG02-07ER41488. We thank D. Neely, P. Foster, and J. Green for providing spectral response of the scintillator, the OSIRIS consortium (UCLA/IST) for use of OSIRIS, K. Kusche, and the ATF technical staff for experimental assistance and A. E. Dangor and L. Willingale for useful discussions.

[1] S. J. Gitomer *et al.*, Phys. Fluids **29**, 2679 (1986).
[2] E. L. Clark *et al.*, Phys. Rev. Lett. **85**, 1654 (2000).
[3] R. Snavely *et al.*, Phys. Rev. Lett. **85**, 2945 (2000).
[4] S. Wilks *et al.*, Phys. Plasmas **8**, 542 (2001); P. Mora, Phys. Rev. Lett. **90**, 185002 (2003).
[5] E. Clark *et al.*, Phys. Rev. Lett. **84**, 670 (2000).
[6] J. Fuchs *et al.*, Nature Phys. **2**, 48 (2006); J. Schreiber *et al.*, Phys. Rev. Lett. **97**, 045005 (2006).
[7] B. Hegelich *et al.*, Nature (London) **439**, 441 (2006); H. Schwoerer *et al.*, Nature (London) **439**, 445 (2006).
[8] T. Toncian *et al.*, Science **312**, 410 (2006).
[9] T. Esirkepov *et al.*, Phys. Rev. Lett. **92**, 175003 (2004).
[10] A. P. L. Robinson *et al.*, New J. Phys. **10**, 013021 (2008).
[11] T. V. Liseykina *et al.*, Plasma Phys. Controlled Fusion **50**, 124033 (2008).
[12] B. Qiao *et al.*, Phys. Rev. Lett. **102**, 145002 (2009); A. Macchi, S. Veghini, and F. Pegoraro, Phys. Rev. Lett. **103**, 085003 (2009).
[13] S. C. Wilks *et al.*, Phys. Rev. Lett. **69**, 1383 (1992).
[14] L. Silva *et al.*, Phys. Rev. Lett. **92**, 015002 (2004); M. Q. He *et al.*, Phys. Rev. E **76**, 035402 (2007); M. Chen *et al.*, Phys. Plasmas **14**, 053102 (2007); A. Henig *et al.*, Phys. Rev. Lett. **102**, 095002 (2009).
[15] A. Henig *et al.*, Phys. Rev. Lett. **103**, 245003 (2009).
[16] M. Kaluza *et al.*, Phys. Rev. Lett. **93**, 045003 (2004).
[17] L. Willingale *et al.*, Phys. Rev. Lett. **96**, 245002 (2006).
[18] T. Esirkepov, M. Yamagiwa, and T. Tajima, Phys. Rev. Lett. **96**, 105001 (2006); L. Willingale *et al.*, IEEE Trans. Plasma Sci. **36**, 1825 (2008).
[19] A. Macchi *et al.*, Phys. Rev. Lett. **94**, 165003 (2005).
[20] R. A. Fonseca, *Lecture Notes in Computer Science* (Springer, Heidelberg, 2002), Vol. III-342, p. 2329.
[21] G.-Z. Sun *et al.*, Phys. Fluids **30**, 526 (1987).